Biophysical Chemistry 184 (2013) 22–28

Contents lists available at ScienceDirect

Biophysical Chemistry

journal homepage: http://www.elsevier.com/locate/biophyschem

Calorimetric studies of the interactions of linker histone $H1^0$ and its carboxyl ($H1^0$–C) and globular ($H1^0$–G) domains with calf-thymus DNA

V.R. Machha [a], J.R. Waddle [a], A.L. Turner [a], S. Wellman [b], V.H. Le [a], E.A. Lewis [a,*]

[a] Department of Chemistry, Mississippi State University, Box 9573, Mississippi State, MS 39762, United States
[b] Department of Pharmacology and Toxicology, University of Mississippi Medical Center, 2500 North State Street, Jackson, MS 39216-4505, United States

GRAPHICAL ABSTRACT

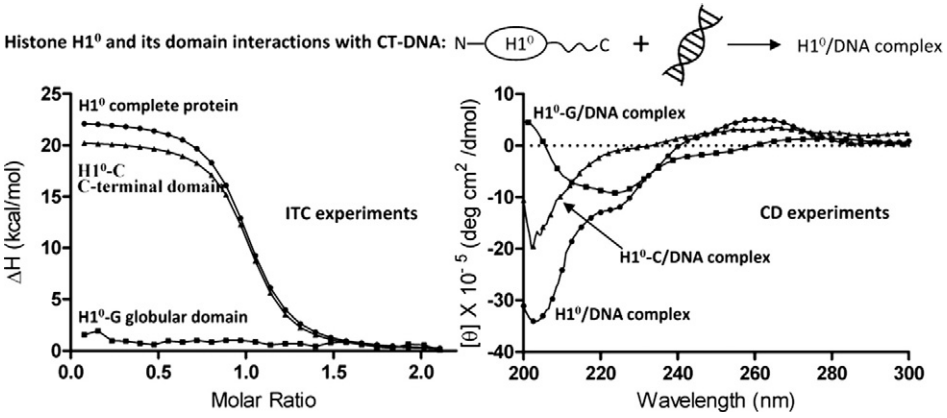

ARTICLE INFO

Article history:
Received 19 June 2013
Received in revised form 8 August 2013
Accepted 12 August 2013
Available online 31 August 2013

Keywords:
Histone
$H1^0$
$H1^0$–C
$H1^0$–G
CT-DNA
Chromatin

ABSTRACT

Histone H1 is a chromatin protein found in most eukaryotes. ITC and CD have been used to study the binding of $H1^0$ and its C-terminal, $H1^0$–C, and globular, $H1^0$–G, domains to a highly polymerized DNA. ITC results indicate that $H1^0$ and $H1^0$–C bind tightly to DNA ($K_a \approx 1 \times 10^7$), with an unfavorable ΔH ($\Delta H \approx +22$ kcal/mol) and a favorable ΔS ($-T\Delta S \approx -30$ kcal/mol). Binding $H1^0$–G to DNA at 25 °C is calorimetrically silent. A multiple independent site model fits the ITC data, with the anomaly in the data near saturation attributed to rearrangement of bound H1, maximizing the number of binding sites. CD experiments indicate that $H1^0$/DNA and $H1^0$–C/DNA complexes form with little change in protein structure but with some DNA restructuring. Salt dependent ITC experiments indicate that the electrostatic contribution to binding $H1^0$ or $H1^0$–C is small ranging from 6% to 17% of the total ΔG.

© 2013 Elsevier B.V. All rights reserved.

Abbreviations: ITC, isothermal titration calorimetry; CD, circular dichroism; CT-DNA, calf thymus DNA.

* Corresponding author at: Department of Chemistry, Mississippi State University, 1115 Hand Lab, Box 9573, and Mississippi State, MS 39762, United States. Tel.: +1 662 325 3584.
E-mail address: elewis@chemistry.msstate.edu (E.A. Lewis).

0301-4622/$ – see front matter © 2013 Elsevier B.V. All rights reserved.
http://dx.doi.org/10.1016/j.bpc.2013.08.005

1. Introduction

Linker histones (H1) are the basic proteins in higher eukaryotes that are responsible for the final condensation of chromatin [1]. H1 also plays important role in regulating gene expression. H1 has been described as a transcription repressor as it limits the access of transcriptional factors to DNA [2–7]. Linker histone binds to DNA that enters or exits the nucleosome [8]. Several crystal structures have been published for the nucleosome (histone core/DNA complex) and the interactions of the core histone proteins with DNA are well understood [9–12]. In contrast the location of the linker histone and its interactions with DNA are more poorly understood.

H1 exists as multiple isoforms, with eleven different subtypes identified in mammals to date. Among the eleven subtypes, seven are expressed in somatic cells (H1.1–H1.5, $H1^0$, and H1.X), and four histones are expressed in germ cells: three in sperm (H1t, H1T2, HILS1) and one in oocytes (H1oo) [13]. All of the H1 histone subtypes have a similar structure composed of three separate domains, a short disordered N-terminal domain approximately 35 amino acid residues in length, a central globular winged helix domain approximately 65 residues in length, and a longer disordered C-terminal domain approximately 100 amino acid residues in length [14]. In mammals the sequence of the H1 globular domain is highly conserved while the N- and C-terminal domains are more varied with respect to sequence [15] and amino acid composition [13]. This variability in the terminal domains is thought to be responsible for the functional differences among the subtypes [16].

The C-terminal domain has a unique amino acid composition dominated by Lys (~40%), Ala (~17%), and Pro (~12%). The positively charged residues in the C-domain take part in the neutralization of the linker-DNA phosphate backbone during chromatin condensation [17,18]. It has been reported that not all of the lys/arg residues in the H1 C-terminal domain are equally involved in the stabilization of condensed chromatin and that the change in DNA structure is not simply the result of charge neutralization [19]. The 24 residues located closest to the globular domain (97–121) and the 24 residues located approximately in the middle of the C-terminus (145–169) play the largest role in the condensation and organization of linker-DNA [19]. Although the C-terminal sequence varies with subtype it is the amino acid composition (i.e. 40% lysine content) that is primarily responsible for the interaction of the C-terminal domain and linker-DNA [19]. Although the C-terminal sequence of the various H1 subtypes is variable, all the subtypes have approximately the same charge and a similar characteristic intrinsically disordered structure [20]. It has been reported that the intrinsically disordered C-terminal domain develops some α-helix and/or β-sheet structure upon binding to DNA [21]. It has been proposed that the interactions between the C-domain and linker-DNA influence the orientation of the globular-domain in the H1/DNA complex [22]. In effect the protein and/or DNA conformational changes brought about by the binding of the C-terminal domain to linker-DNA are thought to play a role in determining the interfacial contacts between the H1 G-domain and the nucleosome in chromatin [22–24].

In the present study we have used isothermal titration calorimetry (ITC) to determine the thermodynamics for binding of $H1^0$, $H1^0$–C, and $H1^0$–G to highly polymerized calf-thymus DNA. We have also used circular dichroism (CD) to evaluate whether the binding of the complete H1 protein ($H1^0$) or its domain peptides ($H1^0$–C and $H1^0$–G) to ds-DNA is accompanied by a change in structure of the protein, protein fragment, or DNA. In our ITC studies, we found that the intact protein ($H1^0$) and its C-terminal domain ($H1^0$–C) bind to CT-DNA with approximately the same affinity ($K_a \approx 1 \times 10^7$). We also observed a surprisingly large endothermic enthalpy change for the formation of these H1/DNA complexes ($\Delta H \approx +22$ kcal/(mol $H1^0$ or $H1^0$–C)). There was no ITC signal for the addition of $H1^0$–G to CT-DNA indicating that either $H1^0$–G binding did not occur or that the $H1^0$–G/DNA complex was formed with a very small change in enthalpy ($\Delta H \approx 0$ kcal/(mol $H1^0$–G)). The $H1^0$/DNA and $H1^0$–C/DNA complexes are driven by a very favorable entropy change ($-T\Delta S \approx -30$ kcal/mol), and the binding site sizes for $H1^0$ and $H1^0$–C were determined to be 36 bp and 28 bp, respectively. Our CD results indicate that CT-DNA is restructured upon complex formation with either the full length H1 protein ($H1^0$) or its C-terminal domain ($H1^0$–C). In contrast, the structure of $H1^0$ is largely unchanged in the DNA complex. Even though the ITC does not detect a binding interaction between the globular domain, $H1^0$–G, and CT-DNA, the CD experiments show a significant change in the $H1^0$–G spectrum in the DNA complex, a sure indication of a strong interaction between $H1^0$–G and DNA. The CD results are consistent with significant loss of α-helical structure in the globular domain as it binds to DNA. These results are discussed in more detail in the Results and Discussion sections of the paper.

2. Materials and methods

2.1. Proteins and DNA samples

The $H1^0$ intact protein and its C-terminal and globular domains were expressed using a bacterial strain of *Escherichia coli* (*Rosetta2* (*De3*) *pLysS*) transformed with a pET-11d (Novagen) expression vector as described [25]. The constructions of the expression strains, induction, extraction, and purification have been described [25,26]. The pure protein fractions were lyophilized using a Savant SPD 111 V Speed-Vac system for 4 h at 35 °C and dissolved in 2 mL of sample buffer. Typically the sample buffer was BPES which is 30 mM K_2HPO_4/KH_2PO_4 (pH = 7.0), 1 mM EDTA, and 100 mM KCl. For the salt dependent studies the amount of added supporting electrolyte, KCl, was 0.0 mM, 30 mM, 70 mM, 130 mM and 290 mM, for the 0.03, 0.06, 0.10, 0.16 and 0.32 M [K^+] solutions respectively. Calf thymus DNA type I was purchased from Sigma (St. Louis, USA) and dissolved in 1 mL of the sample buffer. Both protein and DNA stock solutions were exhaustively dialyzed against the sample buffer (24 h) at 4 °C. DNA concentrations in base pairs (bp) were determined using measured absorbance at 260 nm and a molar extinction coefficient of $\varepsilon_{260} = 1.31 \times 10^4$ bp M^{-1} cm^{-1} [27]. The concentrations of $H1^0$, $H1^0$–C and $H1^0$–G were calculated using extinction coefficients 27.8, 31.1, and 28.6 mL mg^{-1} cm^{-1}, respectively at 205 nm [25].

The approximate molecular weights for the H1 and H1 domain constructs were estimated from their sequences using the ExPASy ProtParam tool (http://web.expasy.org/protparam): Mw ($H1^0$) ≈20.8 kDa, Mw ($H1^0$–C) ≈9.55 kDa, and Mw ($H1^0$–G) ≈9.28 kDa. The approximate average molecular weight of the CT-DNA was 8.42×10^3 kDa (Sigma, St. Louis, USA).

2.2. ITC

Isothermal titration calorimetry (ITC) experiments were performed using a Microcal VP-ITC (Northampton, MA, USA). Titrations were done at five salt concentrations (0.03, 0.06, 0.1, 0.16, and 0.32 M [K^+]) and at 25 °C. All titrations were performed by overfilling the ITC cell with approximately 1.5 mL of a dilute CT-DNA solution (nominally 480 μM in bp). Approximately 250 μL of a dilute solution of $H1^0$, $H1^0$–C, or $H1^0$–G (nominally 150 μM) was titrated into the calorimeter cell. The injection volume in these titrations was nominally 10 μL and a typical titration involved the addition of 25 injections of titrant at 600 second intervals. The 1.5 mL added to the VP ITC cell overfills the cell so that there are no air bubbles in the chamber. As a volume of titrant ($H1^0$, $H1^0$–C, or $H1^0$–G) is added, an equivalent volume of solution is displaced from the cell and titrate concentration is corrected for material loss at each point in the titration. All of our ITC experiments were performed in triplicate at 25 °C. The integrated heat/injection data were fit to an appropriate thermodynamic model using CHASM data analysis software developed in our laboratory [28]. The non-linear regression fitting process yields best fit parameters for K (or ΔG), ΔH, ΔS, and n.

2.3. CD

CD experiments were performed using an Olis DSM 20 spectropolarimeter (Bogart, GA, USA). CT-DNA and protein solutions were prepared with a nominal absorbance of 0.5 AU in a BPES buffer (10 mM KCl, 30 mM phosphate, 0.1 mM EDTA). The nominal concentrations of both protein and CT-DNA were 1.5 μM and 96 μM in DNA bp, respectively. The H1/DNA complex solutions were prepared to have an approximately 0.5:1 molar ratio between the H1 protein and the DNA binding sites using an approximate site size of 32 bp. This ratio was chosen to avoid the complications that appear near the endpoint in the ITC titrations. We used diluted solutions of both protein and DNA, and used excess moles of DNA to prepare complex samples for the CD experiments to minimize complex aggregation. CD spectra were collected over a wavelength range from 200 to 300 nm (with measurements every 0.5 nm) in a 1 cm path length cuvette at room temperature. The spectra represent the average of three scans which were processed using PRISM software (GraphPad Prism Software, San Diego, CA).

3. Results

3.1. ITC

Fig. 1 shows the typical ITC data for titrations of the $H1^0$ and $H1^0$–C proteins in 0.100 M [K^+] solutions. In these experiments the complete histone $H1^0$ and its C-terminal domain, $H1^0$–C, were titrated into highly polymerized CT-DNA at 25 °C. The ITC thermograms were fit using non-linear regression techniques to a multiple independent site model (one site model) and the average best-fit parameters are listed in Table 1. We also attempted to fit these titration data to a nearest neighbor exclusion model [29], however, the multiple sites do not appear to be interacting and do not exhibit either positive or negative cooperativity. This was determined from the independence of ΔH on degree of saturation, ($\Delta h \approx 0.0$). ITC data indicate that although $H1^0$ or $H1^0$–C has a high binding affinity ($KK \approx 10^7\ M^{-1}$) for CT-DNA, the enthalpy change is very unfavorable ($\Delta H \approx +22$ kcal/(mol $H1^0$ or $H1^0$–C)) and complex formation is driven by a large favorable entropy change ($-T\Delta S \approx -30$ kcal/mol). The maximum in the endothermic heat observed just prior to the endpoint in both ITC titrations (Fig. 1A, B) is attributed to overcoming a steric interaction in which a bound protein is partially occupying two adjacent sites and this protein must be relocated in order to fully populate all of the potential protein binding sites. The additional endothermic heat observed near saturation represents the energy cost of relocating the one or more already bound proteins that are unevenly distributed along the linear lattice of the DNA. In effect as $H1^0$ binds non-specifically (electrostatically) to a long DNA molecule, the placement of the proteins is random and can result in multiple partial binding sites that are vacant. The binding-site size, or the number of base pairs occupied per bound $H1^0$, $H1^0$–C or $H1^0$–G protein, was calculated from the ratio of added protein at the titration endpoint to the total number of DNA base pairs in the calorimeter. Previous studies have reported a binding-site size of 10 DNA base pairs for both $H1^0$ and $H1^0$–C [25]. Our ITC results are more consistent with a larger binding site size, 36 bp for $H1^0$ and 28 bp for $H1^0$–C. The interaction between $H1^0$–G and CT-DNA was also studied by ITC but was observed to be calorimetrically silent at 25 °C.

To further probe the nature of the interactions between $H1^0$ or $H1^0$–C with CT-DNA, we performed a salt dependent study in which the experiments shown in Fig. 1 were repeated in solutions having total [K^+] of 0.03, 0.06, 0.100, 0.160 and 0.320 M. In Fig. 2, we have plotted

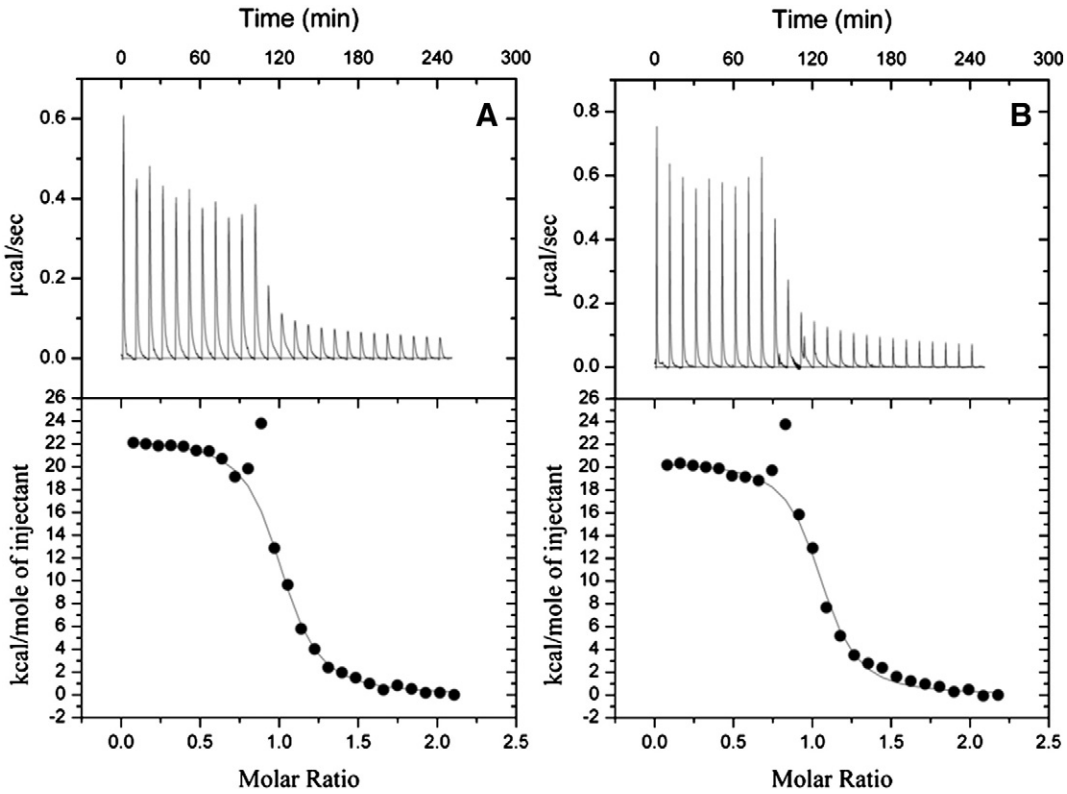

Fig. 1. Panel A shows a typical ITC titration for the addition of $H1^0$ to highly polymerized CT-DNA. The upper half of panel A shows the baseline-corrected raw ITC signal for 25 injections of a dilute $H1^0$ protein solution (10 μL of 150 μM $H1^0$) into the ITC cell filled with a dilute solution of CT-DNA (360 μM bp, 10 μM in $H1^0$ binding sites). The lower half of panel A shows the apparent ΔH for each injection (●) along with the best-fit non-linear regression line (—) for a simple one site binding model. Panel B shows a typical ITC titration for the addition of $H1^0$–C to highly polymerized CT-DNA. The upper half of panel B shows the baseline-corrected raw ITC signal for 25 injections of a dilute $H1^0$–C protein solution (10 μL of 150 μM $H1^0$–C) into the ITC cell filled with a dilute solution of CT-DNA (280 μM bp, 10 μM in $H1^0$–C binding sites). The lower half of panel B shows the ΔH for each injection (●) along with the best-fit non-linear regression line (—) for a simple one site binding model.

Table 1
ITC derived thermodynamic parameters for binding the complete $H1^0$ protein and its carboxyl ($H1^0$–C) and globular domains ($H1^0$–G) to highly polymerized calf thymus DNA.

	K_a (M^{-1}) $\times 10^{-6}$	ΔG (kcal/mol)	ΔH (kcal/mol)	−TΔS (kcal/mol)	Binding site size (bp)
$H1^0$	7.15 ± 0.16	−9.35	21.79 ± 0.19	−31.14	36
$H1^0$–C	7.54 ± 0.14	−9.38	20.61 ± 0.23	−29.99	28
$H1^0$–G	ND	ND	ND	ND	ND

All ITC experiments were performed in triplicate in 100 mM [K^+] BPES buffer at pH 7.0 and 25 °C. The integrated heat/injection data were fit for a one site thermodynamic model using CHASM data analysis software developed in our laboratory [28]. Errors listed are the standard deviations for the best fit parameters K and ΔH determined in triplicate experiments. Effective binding site size in base pairs was calculated from the titration endpoint, the DNA concentration in base pairs and the assumption that saturation stoichiometry is 1:1 (H1: DNA sites).

the values for ΔG, ΔH, and −TΔS for binding $H1^0$ to CT-DNA as a function of the potassium ion concentration. In looking at this plot, it is obvious that increasing the salt concentration results in a continuous but small weakening of the protein/DNA affinity. This plot presents a classic case of enthalpy–entropy compensation wherein larger changes in ΔH are compensated for by the opposite change in the −TΔS term. We also show in Fig. 3 a plot of log K_a vs. the log of the potassium ion concentration. The salt dependence of the K_a for binding $H1^0$ and $H1^0$–C to CT-DNA has been analyzed by the polyelectrolyte theory of Record et al. [30]. Both $H1^0$ and $H1^0$–C exhibit a similar predictable decrease in affinity with increasing ionic strength. The data in Fig. 3 were used to estimate values for $-Z\psi$, i.e. the slopes of the two lines shown in Fig. 3 for the salt dependence of K_a for binding $H1^0$ and $H1^0$–C to CT-DNA. The polyelectrolyte effect on the free energy for binding these proteins to CT-DNA was calculated using Eqs. (1), (2) and (3)

$$\log K_{obs} = \log K_t - Z\psi \log[K^+] \quad (1)$$

$$\Delta G_{pe} = -Z\psi RT \ln[K^+] \quad (2)$$

$$\Delta G_{calc} = \Delta G_t + \Delta G_{pe} \quad (3)$$

where; K_{obs} is the ITC determined value for K_a, and K_t is the non-electrolyte contribution to the overall affinity calculated from the y intercept of the data plotted in Fig. 3. Table 2 lists the values for ΔG_{pe}, the electrostatic contribution to the free energy change, ΔG_t, the non-ionic contribution to the overall binding free energy change and ΔG_{calc},

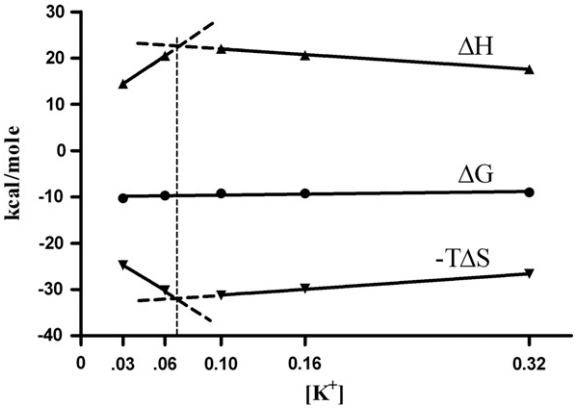

Fig. 2. A plot of the thermodynamic parameters, ΔG, ΔH, and −TΔS for the binding of $H1^0$ to CT-DNA as a function of salt concentration.

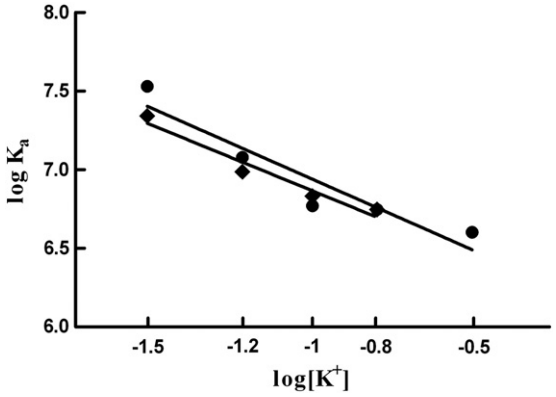

Fig. 3. A plot of log K_a vs log [K^+] for the binding of $H1^0$ and $H1^0$–C to CT-DNA. The data for $H1^0$ are shown as ●, and the data for $H1^0$–C are shown as ♦.

the sum of ΔG_{pe} and ΔG_t, along with the ITC determined value for ΔG for binding either $H1^0$ or $H1^0$–C to CT-DNA, ΔG_{obs}. These calculations were done at as many as five salt concentrations. The polyelectrolyte effect reduces the affinity at higher salt concentrations, a clear indication that an attractive ligand charge/DNA charge interaction is at least partially responsible for the protein's affinity for DNA. However, the polyelectrolyte contribution to the affinity is very small, ranging from only 17.8% for binding $H1^0$ in 0.03 M [K^+] solution to as low as 6% for binding $H1^0$–C in 0.320 M [K^+].

3.2. CD

CD experiments were used to detect any structural changes in the DNA or in the complete H1 protein ($H1^0$) or its domain peptides ($H1^0$–C and $H1^0$–G) upon complex formation. Fig. 4A shows the representative CD spectra for the complete $H1^0$ protein, CT-DNA, and a 0.5:1 protein/CT-DNA complex. (Figs. 5A and 6A show the same spectra for $H1^0$–C and $H1^0$–G and their complexes with CT-DNA.) Fig. 4B again shows the complex spectrum for $H1^0$/CT-DNA, as well as two calculated spectra: 1) the summation of the CD spectra for free $H1^0$ and free CT-DNA and 2) the difference spectrum obtained by subtracting the summation spectrum from the actual spectrum for the complex. From the data shown in Fig. 4A it is clear that both $H1^0$ and CT-DNA exhibit significant structure. The CT-DNA spectrum shows a positive molar ellipticity at 280 nm and a negative molar ellipticity in the vicinity of 245 nm. The DNA spectrum is consistent with CD spectra previously reported for CT-DNA [31,32]. The CD spectrum obtained here for $H1^0$ very closely resembles the CD spectrum reported for H1 by Barbero et al. [33]. Our

Table 2
Parsing the free energy change: calculation of the electrostatic and non-electrostatic contributions to the ΔG for binding $H1^0$ and $H1^0$–C to CT-DNA.

	[K^+]	ΔG_{pe}[a] (kcal/mol)	ΔG_t[b] (kcal/mol)	ΔG_{calc}[c] (kcal/mol)	ΔG_{obs}[d] (kcal/mol)	Ionic contribution[e]
$H1^0$	0.030	−1.8	−8.2	−10.0	−10.3	17.8%
	0.060	−1.5	−8.2	−9.7	−9.7	15.5%
	0.100	−1.2	−8.2	−9.4	−9.2	12.8%
	0.160	−1.0	−8.2	−9.2	−9.2	10.8%
	0.320	−0.6	−8.2	−8.8	−9.0	6.8%
$H1^0$–C	0.030	−1.7	−8.2	−9.9	−9.9	17.5%
	0.060	−1.4	−8.2	−9.6	−9.5	14.5%
	0.100	−1.1	−8.2	−9.3	−9.3	11.8%
	0.160	−0.9	−8.2	−9.1	−9.2	9.8%

[a] The polyelectrolyte contribution to ΔG and ΔG_{pe} was calculated from Eq. (2).
[b] The non-ionic contribution to ΔG and ΔG_t was calculated from Eq. (1).
[c] The calculated value for ΔG is the sum of ΔG_t and ΔG_{pe} (Eq. (3)).
[d] The value for ΔG_{obs} is from the ITC results.
[e] The percent ionic contribution was calculated from $\Delta G_{pe}/\Delta G_{calc}$.

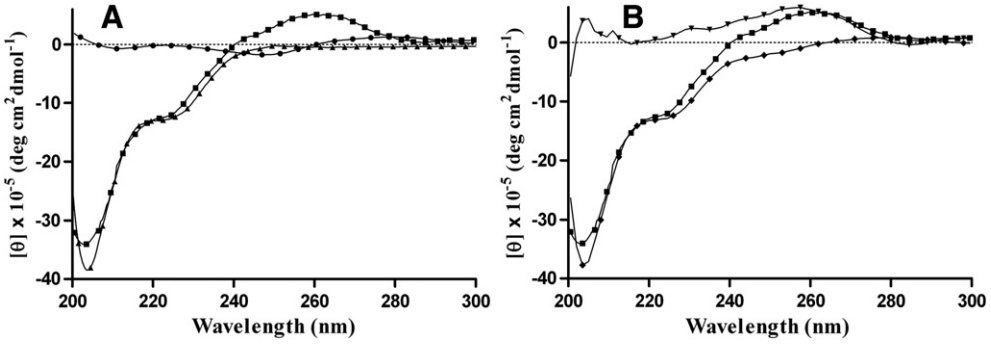

Fig. 4. Panel A shows the CD spectra for the complete protein $H1^0$ (▲), CT-DNA (●), and the partially saturated $H1^0$/CT-DNA complex (■). Panel B shows the CD spectrum for the complex (-■-) along with the calculated summation (♦) and difference (▼) spectra.

$H1^0$ spectrum also closely resembles the CD spectrum reported for H5 by Carter and van Holde [34] and it is consistent with the structural contributions of the globular domain, $H1^0$–G. We estimate that approximately 31% of the $H1^0$ residues are in α-helices and 13% of the $H1^0$ residues are in β-turns, while $H1^0$–C is completely disordered and $H1^0$–G has approximately 70% of its residues in α-helices and 30% of its residues in β-turns in agreement with Cerf et al. [35]. The structure found here for $H1^0$ exceeds the estimates of 8–9% α-helices and 3–4% β-turns reported previously [33]. Nevertheless, it is clear from the spectrum for the $H1^0$/CT-DNA complex in Fig. 4A and the calculated spectra shown in Fig. 4B that the DNA structure is dramatically changed in the $H1^0$/DNA complex while the $H1^0$ structure remains relatively unchanged. Specifically the DNA peak at approximately 280 nm is completely lost. The DNA negative ellipticity at approximately 245 nm is canceled out by the protein positive ellipticity in the same wavelength range. In contrast, the characteristic CD spectrum for the protein is almost unchanged especially over the 200 to 230 nm range in the complex. Clearly the $H1^0$ α-helix and β-turn structure persist in the $H1^0$/CT-DNA complex.

Fig. 5A shows the representative CD spectra for the C-terminal domain $H1^0$–C, CT-DNA, and a 0.5:1 $H1^0$–C/DNA complex. Fig. 5B again shows the complex spectrum for $H1^0$–C/CT-DNA, as well as two calculated spectra: 1) the summation of the CD spectra for free $H1^0$–C and free CT-DNA and 2) the difference spectrum obtained by subtracting the summation spectrum from the actual complex spectrum. Again, from the data shown in Fig. 5A and B it is clear that the C-terminal domain, $H1^0$–C, is very disordered with a featureless CD spectrum from 220 to 300 nm. It is also clear that $H1^0$–C dramatically changes the structure of the DNA in the $H1^0$–C/CT-DNA complex. Specifically the DNA peak at approximately 280 nm is unchanged in intensity; however, the DNA trough at 245 nm is completely lost with the complex ellipticity at 245 nm being much greater than the sum of the $H1^0$–C and DNA features at this wavelength. Although in this case, it is difficult to determine whether the increase in structure of the complex, as evident from the increase in ellipticity at wavelengths above 245 nm, is due to a change in the structure of the bound protein, the complexed DNA, or both.

Fig. 6A shows the representative CD spectra for the globular domain, $H1^0$–G, CT-DNA, and a 0.5:1 $H1^0$–G/CT DNA complex. Fig. 6B again shows the complex spectrum for $H1^0$–G/CT-DNA, as well as two calculated spectra: 1) the summation of the CD spectra for $H1^0$–G and CT-DNA and 2) the difference spectrum obtained by subtracting the summation spectrum from the actual complex spectrum. From the data shown in Fig. 6A and B it is clear that the G-terminal domain, $H1^0$–G, is highly structured with approximately 70% α-helices and 30% β-turns, which is in agreement with the previously reported CD spectra [35]. The spectrum for the $H1^0$–G/CT-DNA complex (shown in Fig. 6A) exhibits significantly reduced ellipticity in the region between 210 and 222 nm, indicating a conformational change in the globular domain upon binding to DNA.

4. Discussion

Linker histones are known to affect chromatin dynamics at the DNA replication and transcription sites in eukaryotes [36]. While it is known that H1 binds to DNA at the point where it either enters or exits the nucleosome [8], the structure of the linked nucleosome complex and the energetics responsible for H1 binding are relatively unknown. In this study the thermodynamic parameters for the binding of intact linker histone $H1^0$ and its globular ($H1^0$–G) and C-terminal ($H1^0$–C) domains to DNA have been determined. The real surprise in the energetics is that the enthalpy change for formation of the $H1^0$/DNA or the $H1^0$–C/DNA complex is very unfavorable ($\Delta H \approx +22$ kcal/(mol H1)) and that $H1^0$/DNA complex formation is driven by a very large change in entropy ($-T\Delta S \approx -30$ kcal/(mol H1)). We have also determined that the interactions between $H1^0$ (or its globular and C-terminal domains) and

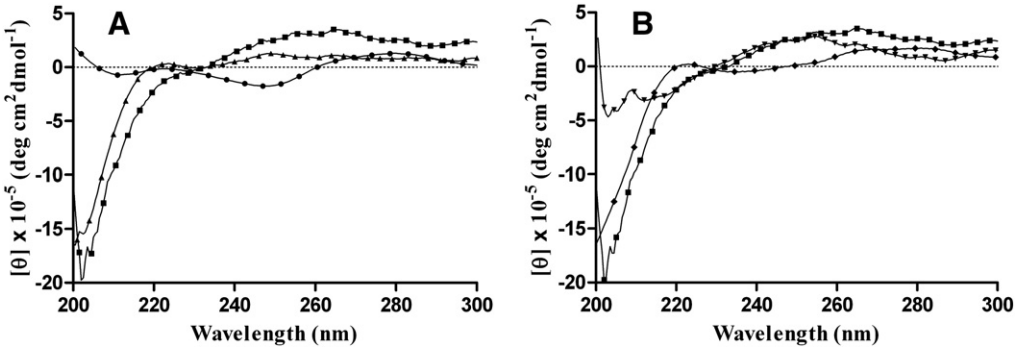

Fig. 5. Panel A shows the CD spectra for the complete protein $H1^0$—C (▲), CT-DNA (●), and the partially saturated $H1^0$–C/CT-DNA complex (■). Panel B shows the CD spectrum for the complex (■) along with the calculated summation (♦) and difference (▼) spectra.

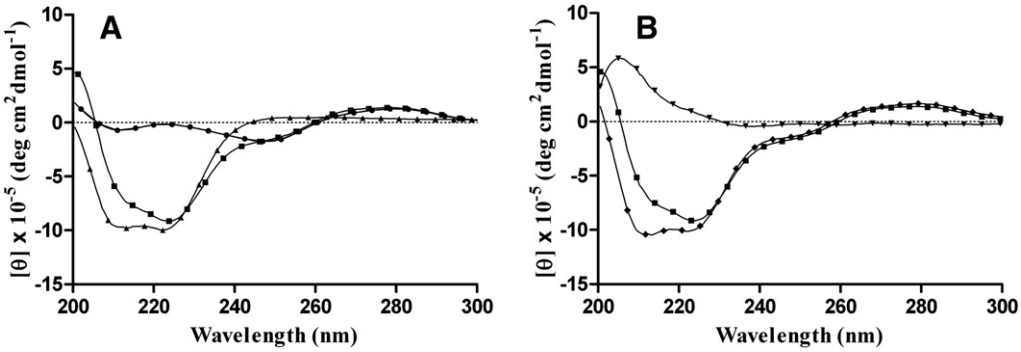

Fig. 6. Panel A shows the CD spectra for the complete protein $H1^0$–G (▲), CT-DNA (●), and the partially saturated $H1^0$–G/CT-DNA complex (■). Panel B shows the CD spectrum for the complex (■) along with the calculated summation (♦) and difference (▼) spectra.

DNA result in subtle changes in either the protein or DNA structure in the H1/DNA complex. All of these results are new and are discussed in detail below.

Fig. 2 presents a classic example of isothermal enthalpy–entropy compensation driven by changes in ionic strength. At the lowest salt concentrations (0.03 and 0.06 M), the absolute values of the enthalpy and entropy change terms, $|\Delta H|$ and $|-T\Delta S|$, for binding $H1^0$ to CT-DNA increase with increasing salt concentration. Upon further increases in the salt concentration, the trend is reversed and the absolute values of the enthalpy and entropy change terms, $|\Delta H|$ and $|-T\Delta S|$, for binding $H1^0$ to CT-DNA decrease with increasing salt concentration. Overall, the absolute value of the free energy change, $|\Delta G|$ decreases monotonically and linearly with increasing salt concentration. There are several references in the literature that indicate that buffers containing 0.07 M $[K^+]$ or $[Na^+]$ are ideal for the study of protein DNA interactions [37–39]. Coincidentally that is approximately the salt concentration where we see a break (0.068 M $[K^+]$) in our plots of ΔH and $-T\Delta S$ vs. $[K^+]$ as shown in Fig. 2. We are not prepared to speculate on the significance of the observation but find it interesting enough to point out this result.

ITC studies demonstrated that the binding of complete protein ($H1^0$) and its C-terminal domain ($H1^0$–C) to CT-DNA was accompanied by a large unfavorable enthalpy change which is compensated by an even larger favorable entropy change. The ITC results for the addition of $H1^0$–G into CT-DNA exhibit no significant heat of interaction (results not shown). This suggests that either the $H1^0$–G/DNA complex does not form (under the conditions of these experiments) or more likely that the complex forms with a very small or near zero change in enthalpy ($\Delta H \approx 0$ kcal/(mol $H1^0$–G)) at 25 °C. The large positive ΔS and positive ΔH terms for the interaction of $H1^0$ or $H1^0$–C are consistent with changes in the structure of the protein or DNA and/or the release of ordered water molecules or ions from the DNA backbone and grooves or from the protein upon complex formation with either $H1^0$ or $H1^0$–C. Our CD results appear to rule out any significant macromolecule structural change contributions to the large positive ΔS term. The slopes, $-Z\psi$, from the salt dependence data shown in Fig. 3, i.e. a plot of log K_a vs log $[K^+]$, indicate that the number of ions released upon H1/DNA complex formation is very small (<1) [30]. The $-Z\psi$ values determined for binding $H1^0$ or $H1^0$–C to linear high molecular weight DNA are −0.89 and −0.82 respectively. In combination, these results point to the loss of bound water as the primary source of the large positive ΔS term. Using Eq. (1) and the data in Fig. 3, we have parsed the free energy change into electrostatic, ΔG_{pe}, and non-electrostatic, ΔG_t, contributions. These data including the calculated and observed values for ΔG are listed in Table 2. The agreement between the ΔG_{obs} and ΔG_{calc} is excellent and the electrostatic contribution to the overall free energy change varies from a maximum of 17% at 0.03 M $[K^+]$ to a low of 6% at 0.320 M $[K^+]$. The largest electrostatic contributions to the overall free energy are observed as expected at the lowest salt concentrations and the smallest electrostatic contributions to the overall free energy change are observed at the highest salt concentrations.

We have used a multiple equivalent site model to fit the ITC titration data. We used polyelectrolyte theory, and the ITC equations developed by Velazquez-Campoy to rule out neighboring site interactions [29,30]. In effect, the linear DNA is simply represented here as a continuous lattice of non-interacting binding sites. We have used the ITC endpoints and the concentrations of the titrant (ligand or protein) and the titrate (DNA bp) to calculate the binding site sizes for $H1^0$ and $H1^0$–C. Whether a binding site is fully covered by bound protein remains a question. What is known is that there is no interaction between adjacent sites and the value of the interaction enthalpy parameter, Δh, is zero [29]. One anomaly that is observed in the thermograms for the titration of CT-DNA with either $H1^0$ or $H1^0$–C is a more endothermic peak in the thermogram that is seen just before the DNA is saturated with protein. This effect is shown in Fig. 7 which includes a fit for the multiple equivalent site model (one site model), a fit for a two non-equivalent site model, and an area above the equivalent site model line that represents the enthalpy change for rearrangement of bound H1 near saturation. The two non-equivalent sites show very high uncertainty in the second site parameters as it is based mostly on a single data point and the rearrangement reaction cannot be fit as a function of added ligand. In actuality, the overall binding process is discontinuous in that the rearrangement reaction only occurs after a critical point is reached in the titration. The rearrangement of bound H1, perhaps a sliding of H1 along the DNA, comes at a cost in ΔH of approximately7.5 kcal/mol. Binding of the complete $H1^0$ protein or its C-terminal peptide to ds-DNA is non-specific (i.e. the protein does not target a specific DNA sequence or region) [40]. As the protein (or peptide) concentration approaches DNA saturation, randomly bound protein must be "rearranged" along the DNA in order to minimize the number of partially obscured H1 binding sites and thereby maximize the number of

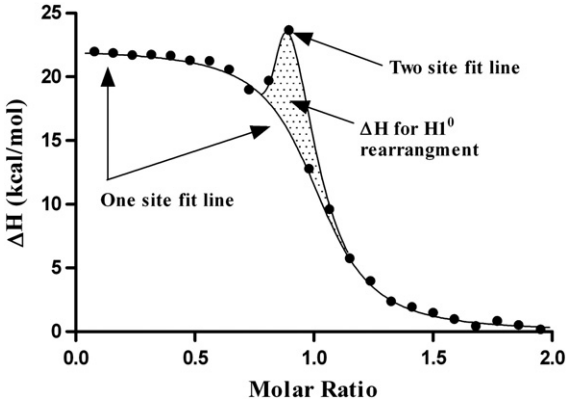

Fig. 7. ITC data for the addition of $H1^0$–C to CT-DNA. These are the same data that were shown in Fig. 1B, fit to two different thermodynamic models, a one site model and a two site model that incorporates the rearrangement reaction for data approaching the endpoint. The shaded area represents the heat for the rearrangement of bound protein.

available protein binding sites. This implies that all sites are filled with no overlap of the protein or peptide between adjacent binding sites. This observation is consistent with a recently published small angle X-ray diffraction study which revealed that H1 binding to DNA is a two-step process [41]. The first step, the non-specific electrostatic interaction between the poly-cationic H1 and poly-anionic DNA leads to the formation of primary assemblies having long columnar hexagonal structure. The second step, the successive rearrangement of H1 molecules in the formed assemblies, results in shorter columnar hexagonal structures [41].

CD results indicate that the two peaks attributed to CT-DNA, i.e. 245 and 280 nm, were both attenuated upon formation of the $H1^0$/CT-DNA (or $H1^0$–C/CT-DNA) complex. This is consistent with a conformational change in DNA that is induced by $H1^0$ or $H1^0$–C binding. This result is consistent with several previous studies which have suggested that binding the H1 C-terminal domain to DNA causes bending of chromatosomal DNA to facilitate a stem-like structure [42,43]. In the case of the globular domain, the CD results indicate that the binding of $H1^0$–G to CT-DNA causes a significant decrease in negative ellipticity between 210 and 222 nm, not only suggesting that there is a strong interaction between $H1^0$–G and CT-DNA, but that there is also some unfolding of the globular domain as it binds to DNA. These CD results also indicate that binding of $H1^0$–G to CT-DNA has no detectable effect on the DNA conformation in the complex.

In conclusion, this study clearly shows that high affinity complexes are formed between $H1^0$ and $H1^0$–C with CT-DNA. The formation of these protein (or peptide) DNA complexes is driven primarily by large favorable entropy changes. It would appear that these large positive entropy changes must result primarily from the expulsion of bound water molecules from the binding interface.

References

[1] L.M. Carruthers, J. Bednar, C.L. Woodcock, J.C. Hansen, Linker histones stabilize the intrinsic salt-dependent folding of nucleosomal arrays: mechanistic ramifications for higher-order chromatin folding, Biochemistry 37 (1998) 14776–14787.
[2] X. Shen, L. Yu, J.W. Weir, M.A. Gorovsky, Linker histones are not essential and affect chromatin condensation in vivo, Cell 82 (1995) 47–56.
[3] F. Thoma, T. Koller, A. Klug, Involvement of histone H1 in the organization of the nucleosome and of the salt-dependent superstructures of chromatin, J Cell Biol 83 (1979) 403–427.
[4] Y. Fan, T. Nikitina, J. Zhao, T.J. Fleury, R. Bhattacharyya, E.E. Bouhassira, A. Stein, C.L. Woodcock, A.I. Skoultchi, Histone H1 depletion in mammals alters global chromatin structure but causes specific changes in gene regulation, Cell 123 (2005) 1199–1212.
[5] G.E. Croston, L.A. Kerrigan, L.M. Lira, D.R. Marshak, J.T. Kadonaga, Sequence-specific antirepression of histone H1-mediated inhibition of basal RNA polymerase II transcription, Science 251 (1991) 643–649.
[6] J. Zlatanova, K. van Holde, Linker histones versus HMG1/2: a struggle for dominance? Bioessays 20 (1998) 584–588.
[7] B.D. Strahl, C.D. Allis, The language of covalent histone modifications, Nature 403 (2000) 41–45.
[8] C.L. Woodcock, Chromatin architecture, Curr. Opin. Struct. Biol. 16 (2006) 213–220.
[9] A. Ramaswamy, I. Bahar, I. Ioshikhes, Structural dynamics of nucleosome core particle: comparison with nucleosomes containing histone variants, Proteins 58 (2005) 683–696.
[10] R.K. Suto, M.J. Clarkson, D.J. Tremethick, K. Luger, Crystal structure of a nucleosome core particle containing the variant histone H2A.Z, Nat. Struct. Biol. 7 (2000) 1121–1124.
[11] C. Zheng, J.J. Hayes, Intra- and inter-nucleosomal protein–DNA interactions of the core histone tail domains in a model system, J. Biol. Chem. 278 (2003) 24217–24224.
[12] L. Marino-Ramirez, M.G. Kann, B.A. Shoemaker, D. Landsman, Histone structure and nucleosome stability, Expert Rev Proteomics 2 (2005) 719–729.
[13] N. Happel, D. Doenecke, Histone H1 and its isoforms: contribution to chromatin structure and function, Gene 431 (2009) 1–12.
[14] J. Allan, P.G. Hartman, C. Crane-Robinson, F.X. Aviles, The structure of histone H1 and its location in chromatin, Nature 288 (1980) 675–679.
[15] M.H. Parseghian, B.A. Hamkalo, A compendium of the histone H1 family of somatic subtypes: an elusive cast of characters and their characteristics, Biochem. Cell Biol. 79 (2001) 289–304.
[16] A. Izzo, K. Kamieniarz, R. Schneider, The histone H1 family: specific members, specific functions? Biol. Chem. 389 (2008) 333–343.
[17] I. Ponte, R. Vila, P. Suau, Sequence complexity of histone H1 subtypes, Mol. Biol. Evol. 20 (2003) 371–380.
[18] J.A. Subirana, Analysis of the charge distribution in the C-terminal region of histone H1 as related to its interaction with DNA, Biopolymers 29 (1990) 1351–1357.
[19] X. Lu, J.C. Hansen, Identification of specific functional subdomains within the linker histone H10 C-terminal domain, J. Biol. Chem. 279 (2004) 8701–8707.
[20] X. Lu, B. Hamkalo, M.H. Parseghian, J.C. Hansen, Chromatin condensing functions of the linker histone C-terminal domain are mediated by specific amino acid composition and intrinsic protein disorder, Biochemistry 48 (2009) 164–172.
[21] J.C. Hansen, X. Lu, E.D. Ross, R.W. Woody, Intrinsic protein disorder, amino acid composition, and histone terminal domains, J. Biol. Chem. 281 (2006) 1853–1856.
[22] T. Misteli, A. Gunjan, R. Hock, M. Bustin, D.T. Brown, Dynamic binding of histone H1 to chromatin in living cells, Nature 408 (2000) 877–881.
[23] P. Vyas, D.T. Brown, N- and C-terminal domains determine differential nucleosomal binding geometry and affinity of linker histone isotypes H1(0) and H1c, J. Biol. Chem. 287 (2012) 11778–11787.
[24] E.M. George, T. Izard, S.D. Anderson, D.T. Brown, Nucleosome interaction surface of linker histone H1c is distinct from that of H1(0), J. Biol. Chem. 285 (2010) 20891–20896.
[25] N.M. Mamoon, Y. Song, S.E. Wellman, Histone H10 and its carboxyl-terminal domain bind in the major groove of DNA, Biochemistry 41 (2002) 9222–9228.
[26] S.E. Wellman, Y. Song, D. Su, N.M. Mamoon, Purification of mouse H1 histones expressed in *Escherichia coli*, Biotechnol. Appl. Biochem. 26 (Pt 2) (1997) 117–123.
[27] R.D. Wells, J.E. Larson, R.C. Grant, B.E. Shortle, C.R. Cantor, Physicochemical studies on polydeoxyribonucleotides containing defined repeating nucleotide sequences, J. Mol. Biol. 54 (1970) 465–497.
[28] V.H. Le, R. Buscaglia, J.B. Chaires, E.A. Lewis, Modeling complex equilibria in isothermal titration calorimetry experiments: thermodynamic parameters estimation for a three-binding-site model, Anal. Biochem. 434 (2013) 233–241.
[29] A. Velazquez-Campoy, Ligand binding to one-dimensional lattice-like macromolecules: analysis of the McGhee–von Hippel theory implemented in isothermal titration calorimetry, Anal. Biochem. 348 (2006) 94–104.
[30] M.T. Record Jr., C.F. Anderson, T.M. Lohman, Thermodynamic analysis of ion effects on the binding and conformational equilibria of proteins and nucleic acids: the roles of ion association or release, screening, and ion effects on water activity, Q. Rev. Biophys. 11 (1978) 103–178.
[31] D.M. Gray, A.R. Morgan, R.L. Ratliff, A comparison of the circular dichroism spectra of synthetic DNA sequences of the homopurine. homopyrimidine and mixed purine–pyrimidine types, Nucleic Acids Res. 5 (1978) 3679–3695.
[32] S.Z. Hirschman, G. Felsenfeld, Determination of DNA composition and concentration by spectral analysis, J. Mol. Biol. 16 (1966) 347–358.
[33] J.L. Barbero, L. Franco, F. Montero, F. Moran, Structural studies on histones H1. Circular dichroism and difference spectroscopy of the histones H1 and their trypsin-resistant cores from calf thymus and from the fruit fly *Ceratitis capitata*, Biochemistry 19 (1980) 4080–4087.
[34] G.J. Carter, K. van Holde, Self-association of linker histone H5 and of its globular domain: evidence for specific self-contacts, Biochemistry 37 (1998) 12477–12488.
[35] C. Cerf, G. Lippens, S. Muyldermans, A. Segers, V. Ramakrishnan, S.J. Wodak, K. Hallenga, L. Wyns, Homo- and heteronuclear two-dimensional NMR studies of the globular domain of histone H1: sequential assignment and secondary structure, Biochemistry 32 (1993) 11345–11351.
[36] H. Hashimoto, Y. Takami, E. Sonoda, T. Iwasaki, H. Iwano, M. Tachibana, S. Takeda, T. Nakayama, H. Kimura, Y. Shinkai, Histone H1 null vertebrate cells exhibit altered nucleosome architecture, Nucleic Acids Res. 38 (2010) 3533–3545.
[37] M. Read, R.J. Harrison, B. Romagnoli, F.A. Tanious, D.H. Gowan, A.P. Reszka, W.D. Wilson, L.R. Kelland, S. Neidle, Structure-based design of selective and potent G-quadruplex-mediated telomerase inhibitors, Proc. Natl. Acad. Sci. U. S. A. 98 (2001) 4844–4849.
[38] S. Sparapani, S.M. Haider, F. Doria, M. Gunaratnam, S. Neidle, Rational design of acridine-based ligands with selectivity for human telomeric quadruplexes, J. Am. Chem. Soc. 132 (2010) 12263–122272.
[39] L. Tentori, O. Forini, E. Fossile, A. Muzi, M. Vergati, I. Portarena, C. Amici, B. Gold, G. Graziani, N3-methyladenine induces early poly(ADP-ribosylation), reduction of nuclear factor-kappa B DNA binding ability, and nuclear up-regulation of telomerase activity, Mol. Pharmacol. 67 (2005) 572–581.
[40] J. Allan, T. Mitchell, N. Harborne, L. Bohm, C. Crane-Robinson, Roles of H1 domains in determining higher order chromatin structure and H1 location, J. Mol. Biol. 187 (1986) 591–601.
[41] R. Dootz, A.C. Toma, T. Pfohl, Structural and dynamic properties of linker histone H1 binding to DNA, Biomicrofluidics 5 (2011) 24104.
[42] J. Bednar, R.A. Horowitz, S.A. Grigoryev, L.M. Carruthers, J.C. Hansen, A.J. Koster, C.L. Woodcock, Nucleosomes, linker DNA, and linker histone form a unique structural motif that directs the higher-order folding and compaction of chromatin, Proc. Natl. Acad. Sci. 95 (1998) 14173–14178.
[43] J. Zlatanova, C. Seebart, M. Tomschik, The linker-protein network: control of nucleosomal DNA accessibility, Trends Biochem Sci 33 (2008) 247–253.